*Journal of Sound and Vibration* (1999) **225**(1), 3–28
*Article No.* jsvi.1999.2232, available online at http://www.idealibrary.com on IDEAL®

# GROUND VIBRATION GENERATED BY A HARMONIC LOAD ACTING ON A RAILWAY TRACK

X. SHENG

*Civil Engineering Department, East China Jiaotong University Nanchang, Jiangxi*, 330013, *People's Republic of China*

AND

C. J. C. JONES, M. PETYT

*Institute of Sound and vibration Research, University of Southampton, Southampton, SO*17 1*BJ*, *England*

(*Received* 17 *September* 1998, *and in final form* 12 *January* 1999)

A calculation method has been produced for the propagation of vibration in the ground from a stationary oscillating load applied via a railway track structure. The model includes the track as an infinite layered beam structure resting on a ground made up of infinite parallel homogeneous elastic layers. These layers may either be constrained at the lower interface or coupled to an elastic half-space. A similar model, based on wave propagating finite elements, has previously been shown to be useful in predicting the behaviour of real soils and railway tracks, but the applicability of that model was limited by long computation times. The present method is more efficient in calculating the responses at a large number of positions. The development of the theory allows analysis in terms of the amplitudes of different wave types propagating along, and normal to, the track. Example calculations are presented for a ground consisting of a layer on a half-space. By changing only the depth of the layer, two different wave propagation regimes are found, the first where propagation takes place via modes of the layer and the second, where propagation takes place via the bulk waves in the layer and the Rayleigh wave in the substratum. Both examples show the track structure to have a strong effect on the directivity and amplitude of the response of the ground surface.



## 1. INTRODUCTION

Low-frequency, surface-propagating ground vibration from trains is often perceptible in buildings adjacent to the track. This may cause annoyance, sleep disturbance and concern over possible damage to the property. Surface propagating vibration represents a significant environmental impact to be taken into account in the design of new or realigned railways. High vibration levels in the frequency range from about 4 to 50 Hz are especially associated with the operation of heavy-axle freight vehicles [1], however, passenger operations can also cause significant levels. Some railways have reported higher frequency vibration, associated with

0022-460X/99/310003 + 26 $30.00/0 

"ground-borne noise", to be propagated from surface railways as well as from, the more well-known source, trains running in tunnels [1]. In this case, the frequency range of interest is extended to about 200 Hz.

There is a clear need for numerical models in order to study the vibration propagation from railways and to devise new means of attenuating the vibration [2]. For this reason a number of two- and three-dimensional models have been developed by various workers for the study of ground vibration from trains.

In 1991, Jones and Petyt proposed a model for propagation from a railway track which used a two-dimensional representation of the ground, first as a half-space [3], and later as a layer on a half-space [4]. In that work no model of the railway track was included and the load was applied as a constant pressure amplitude acting over a finite width of the ground surface. The dimensionality of the model implies a load of constant value and of infinite length in three dimensions. These models followed the formulation of Kausel and Roësset [5] in the use of exact dynamic stiffness matrices formulated in the frequency-wave number domain for the layer and the half-space. By transforming the formulation for the lateral direction of displacement into the wave number domain, the solution for propagation of waves to infinity is obtained. Parallel layers of different materials are implemented by the discretization in the vertical direction into 'layer-elements' and assembling separate stiffness matrices to form a matrix representing the layered half-space.

A number of other cross-sectional (i.e. two-dimensional) models which allow arbitrary geometry have been used in the study of train-induced ground vibration since the work of Jones and Petyt. However, it is the interest within the present work to follow the development of three-dimensional models so that the influence of the longitudinal properties of the track structure can be taken into account.

In further work by Jones and Petyt, the dynamic stiffness matrix approach for the layer elements was extended to produce a three-dimensional model of the ground as a layered medium [6, 7].

A model with an alternative formulation was used by Jones [2, 8] to produce a three-dimensional model of the ground coupled to a layered beam structure. In this model, instead of exact layer elements, the formulation in the wave number domain was constructed using a finite-element approximation for the variation of displacement with depth. The theory for this model has not been published. However, it followed the approach that was developed by Waas [9] and Tassoulas and Kausel [10] in two dimensions. The three-dimensional layer elements of references [2, 8] used cubic-polynomial shape functions rather than the linear approximation across each layer element of the previous work.

The method of coupling a track and ground structure in references [2, 8] has been used previously for the study of vibration in the 'ground-borne noise' frequency range [11] where a harmonic load at a fixed point on the track is used to predict the effect of design changes to the track. In this model the ground was represented as a three-dimensional half-space. The method of coupling of the track to the ground is published for the first time in the present paper.

In reference [8], the model of the track on the layered ground was shown to be useful in predicting the effects of vibration from heavy freight trains. In the same

paper, but using a separate model of the track with multiple moving loads, the vibration at the track was shown to be a sum of two components; the first generated by the action of the passing of the deformation pattern under the multiple loads of the train, and the second generated dynamically as the unsprung masses of the train pass over the irregular profile of the track-top. For a train moving at a speed well below the wave speeds in the ground, a comparison in reference [8] for a particular case of predicted and measured vibration on the track showed the dynamically induced component to be the more important above about 15 Hz. The three-dimensional coupled track and layered ground model was then used with a forcing function applied at each sleeper position, with a time/phase shift appropriate to the axle spacing and speed of the train, to generate a prediction of the vibration at a distance from the track. This was compared to a measured spectrum. Away from the track the component generated by the movement of the loads was shown to diminish in importance.

Takemiya [12] divides the sources of excitation of vibration from a train into three types of force: (i) a fixed-point dynamic force due to the irregularity of the track (this is an impulse in the time domain), (ii) a moving non-harmonic axle load, and (iii) a moving harmonic load due to irregularities of the wheel and the effects of the vibrational modes of the vehicle suspension. The solution for moving non-oscillatory axle loads (ii) has been pursued by some workers [13, 14] having an interest in the generation of vibration from high-speed trains that approach, and exceed, the wave speeds in the ground. The present authors intend to present a model which addresses the forcing type (iii) in a future paper. Takemiya shows the need for a layered ground model and concludes that a model for the response of a fixed-point excitation is suitable for the study of the excitation (i) and for excitations (ii) and (iii) in the case of slow moving vehicles (i.e. well below the ground wave speeds).

Thus references [8, 12] show that a model in which the loading has a broad band of frequency but is stationary on the track is appropriate for use in a number of studies of ground vibration. This is the subject of the present paper.

The importance of including the effects of layered ground for surface propagation of vibration from railways was demonstrated in reference [2] in the interpretation of experiments. A strong influence of the layered structure of the ground on its propagation characteristics in the frequency range of interest and small variations in the layer depth can lead to significant differences in the level of transmitted vibration. It is also shown in reference [2] that a model in which the ground is represented as a single homogeneous elastic layer overlying a half-space can predict measured transfer response functions of a real ground site. The importance of modelling the ground layers is also emphasized in reference [12].

A limitation on the usefulness of the track and layered ground calculation of references [2, 8] lay in the long computation times. This made it impossible to fully utilize the method in the prediction scheme proposed in reference [8] as it was not possible to generate the large number of transfer response functions from the sleeper locations to a point on the ground.

The work reported in this paper is a continuation of that of references [6–8]. It presents a more efficient calculation method which can be used for loads acting

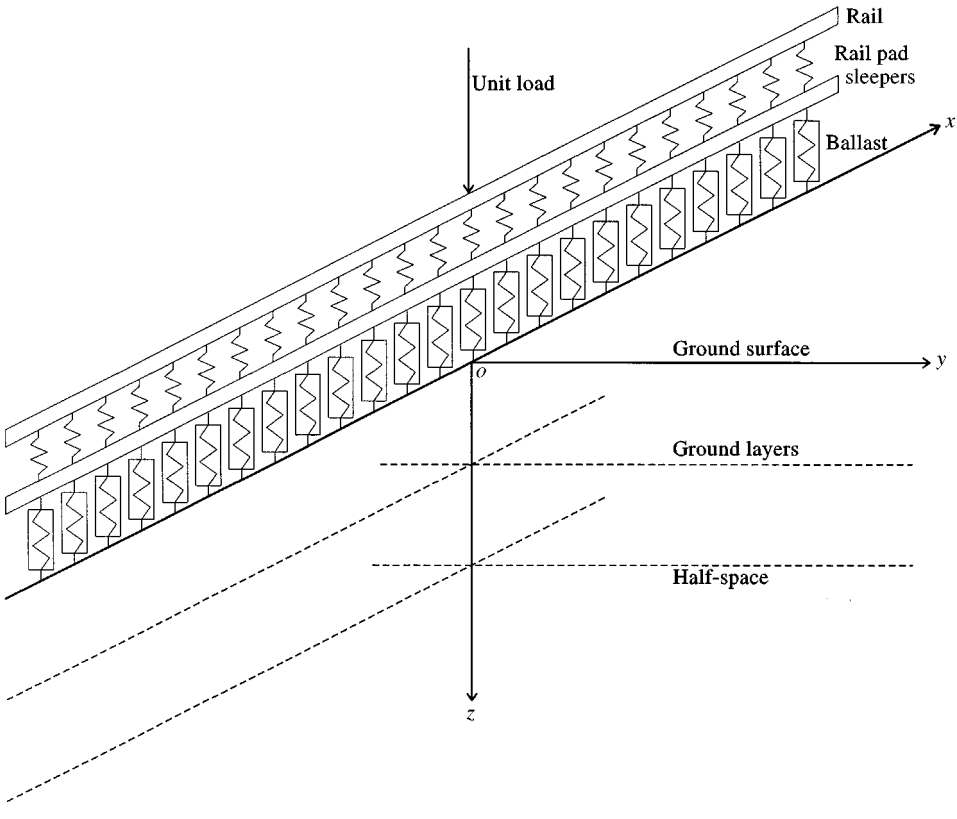


Figure 1. The railway-ground system.

directly on the ground, or, as shown in Figure 1, for a load acting via a coupled track structure. Rather than use either the exact or discretized dynamic stiffness matrix techniques, it has been found in the present work that improved computational efficiency for the problem can be achieved by using the flexibility matrix approach as set out by Haskell [15] and Thomson [16]. The derivation of the flexibility matrix for a three-dimensional ground layer is described for a Cartesian co-ordinate system in section 2 of the paper. With some mathematical treatment, numerical difficulties that occur in a number of the models used in references [2–8] are avoided. An advantage of using the flexibility matrix is that all the matrices being manipulated are of order less than or equal to 6. Axial symmetry in the wave number domain matrix is used in the explicit analytical expression of the formulae, resulting in further improvement of the calculation efficiency and accuracy (section 2.3). Section 2.4 presents the formulae for the ground response when a harmonic load act directly on its surface.

In section 3, the coupling of the railway structure and the ground is achieved through the calculation of a Fourier transformed loading function for the railway. Although the equations for only one particular track construction are presented in this paper, other track structure types can be modelled by simple modifications of the track equations.

Section 4 presents example results showing the effect of the track structure on the vibration response over the surface of the ground.

## 2. THE FOURIER TRANSFORMED DYNAMIC FLEXIBILITY MATRIX OF THE GROUND

### 2.1. DEFINITION OF THE DYNAMIC FLEXIBILITY MATRIX

The model of the track and the ground is represented in Figure 1. Shown there, the plane $Oxy$ stands for the surface of the ground, downward from which, the ground consists of a number, $n$, of parallel layers of different materials. The $n$th layer overlies a half-space or a rigid foundation, which is identified as 'layer' number $(n+1)$. For the $j$th layer the material constants are: elastic modulus, $E_j$, Poisson's ratio, $v_j$, density, $\rho_j$, loss factor, $\eta_j$ and layer thickness, $h_j$. If the $(n+1)$th layer is a half-space, then its material constants are $E_{n+1}$, $v_{n+1}$, $\rho_{n+1}$ and $\eta_{n+1}$.

The steady state displacement amplitudes of point $(x, y, 0)$ on the ground surface in $x, y, z$ directions ($z$-axis is downward into the ground), due to a unit harmonic load $e^{i\omega t}$, where $i = \sqrt{-1}$, $\omega$ is angular frequency, acting at the origin $O$ in the $x$ direction, are denoted by $\delta_{11}, \delta_{21}, \delta_{31}$ respectively. When the unit harmonic load acts at $O$ in the $y$ direction the displacements are denoted, $\delta_{12}, \delta_{22}, \delta_{32}$, and $\delta_{13}, \delta_{23}, \delta_{33}$ when the unit load is in the $z$ direction. A matrix, $[\boldsymbol{\delta}]$, can be defined as

$$[\boldsymbol{\delta}] = \begin{bmatrix} \delta_{11} & \delta_{12} & \delta_{13} \\ \delta_{21} & \delta_{22} & \delta_{23} \\ \delta_{31} & \delta_{32} & \delta_{33} \end{bmatrix} = [\boldsymbol{\delta}(x, y)] \tag{1}$$

This is called the dynamic flexibility matrix of the ground or the displacement Green's function. In general the $\delta$'s are complex.

Now suppose that, on the surface of the ground, the harmonic load distributions $p_x(x, y)e^{i\omega t}$, $p_y(x, y)e^{i\omega t}$, $p_z(x, y)e^{i\omega t}$ act in $x, y, z$ directions respectively. The total steady state vibration amplitudes of point $(x, y, 0)$ in $x, y, z$ directions, denoted by $u_{10}(x, y)$, $v_{10}(x, y)$ and $w_{10}(x, y)$, respectively, are

$$\begin{Bmatrix} u_{10}(x, y) \\ v_{10}(x, y) \\ w_{10}(x, y) \end{Bmatrix} = \begin{Bmatrix} u_{10} \\ v_{10} \\ w_{10} \end{Bmatrix} = \int_{-\infty}^{\infty} \int_{-\infty}^{\infty} [\delta(x - r, y - s)] \begin{Bmatrix} p_x(r, s) \\ p_y(r, s) \\ p_z(r, s) \end{Bmatrix} dr\, ds. \tag{2}$$

Equation (2) is a convolution integration. Using the Fourier transform pairs

$$\bar{f}(\beta) = \int_{-\infty}^{\infty} f(x) e^{-i\beta x} dx, \qquad f(x) = \frac{1}{2\pi} \int_{-\infty}^{\infty} \bar{f}(\beta) e^{i\beta x} d\beta,$$

$$\bar{f}(\beta, \gamma) = \int_{-\infty}^{\infty} \int_{-\infty}^{\infty} f(x, y) e^{-i(\beta x + \gamma y)} dx\, dy,$$

$$f(x, y) = \frac{1}{4\pi^2} \int_{-\infty}^{\infty} \int_{-\infty}^{\infty} \bar{f}(\beta, \gamma) e^{i(\beta x + \gamma y)} d\beta\, d\gamma \tag{3}$$

to transform equation (2) into the domain of the wave numbers $\beta$ in the $x$ direction and $\gamma$ in the $y$ direction, yields

$$\begin{Bmatrix} \bar{u}_{10}(\beta,\gamma) \\ \bar{v}_{10}(\beta,\gamma) \\ \bar{w}_{10}(\beta,\gamma) \end{Bmatrix} = [\bar{\boldsymbol{\delta}}(\beta,\gamma)] \begin{Bmatrix} \bar{p}_x(\beta,\gamma) \\ \bar{p}_y(\beta,\gamma) \\ \bar{p}_z(\beta,\gamma) \end{Bmatrix}, \tag{4}$$

where $\bar{u}_{10}(\beta,\gamma)$ stands for the Fourier transform of $u_{10}(x,y)$, etc. The matrix $[\bar{\boldsymbol{\delta}}(\beta,\gamma)]$ is called the Fourier-transformed dynamic flexibility matrix of the ground. The derivation of an exact expression for this matrix is dealt with below in section 2.2.

## 2.2. DERIVATION OF THE FOURIER-TRANSFORMED DYNAMIC FLEXIBILITY MATRIX

### 2.2.1. *Analysis for a single ground layer*

The steady state displacements in the frequency domain at the point $(x, y, z_j)$ (where $z_j \in (0, h_j)$) are denoted by $u_j(x,y,z_j)\mathrm{e}^{\mathrm{i}\omega t}$, $v_j(x,y,z_j)\mathrm{e}^{\mathrm{i}\omega t}$, $w_j(x,y,z_j)\mathrm{e}^{\mathrm{i}\omega t}$, where $u_j(x,y,z_j)$, $v_j(x,y,z_j)$ and $w_j(x,y,z_j)$ are generally complex numbers and their Fourier transforms, i.e., in the wave number domain, are denoted by $\bar{u}_j(\beta,\gamma,z_j)$, $\bar{v}_j(\beta,\gamma,z_j)$, $\bar{w}_j(\beta,\gamma,z_j)$. Put

$$\begin{aligned} \{\bar{\mathbf{u}}\}_{j0} &= (\bar{u}_j(\beta,\gamma,0), \bar{v}_j(\beta,\gamma,0), \bar{w}_j(\beta,\gamma,0))^{\mathrm{T}}, \\ \{\bar{\mathbf{u}}\}_{j1} &= (\bar{u}_j(\beta,\gamma,h_j), \bar{v}_j(\beta,\gamma,h_j), \bar{w}_j(\beta,\gamma,h_j))^{\mathrm{T}}, \end{aligned} \tag{5}$$

where $\{\bar{\mathbf{u}}\}_{j0}$ stands for the Fourier transform of the displacement vector of the top interface of the $j$th layer, and $\{\bar{\mathbf{u}}\}_{j1}$ for the Fourier transform of displacement vector of the bottom interface of the $j$th layer.

The three components of stresses in $x$, $y$, $z$ directions on the top of the $j$th layer are $\tau_{xzj}(x,y,0)\mathrm{e}^{\mathrm{i}\omega t}$, $\tau_{yzj}(x,y,0)\mathrm{e}^{\mathrm{i}\omega t}$, $\tau_{zzj}(x,y,0)\mathrm{e}^{\mathrm{i}\omega t}$, and those at the bottom are $\tau_{xzj}(x,y,h_j)\mathrm{e}^{\mathrm{i}\omega t}$, $\tau_{yzj}(x,y,h_j)\mathrm{e}^{\mathrm{i}\omega t}$, $\tau_{zzj}(x,y,h_j)\mathrm{e}^{\mathrm{i}\omega t}$. The Fourier transforms of the stress vectors at the top and bottom of the $j$th layer are then defined as

$$\begin{aligned} \{\bar{\boldsymbol{\tau}}\}_{j0} &= (\bar{\tau}_{xzj}(\beta,\gamma,0), \bar{\tau}_{yzj}(\beta,\gamma,0), \bar{\tau}_{zzj}(\beta,\gamma,0))^{\mathrm{T}}, \\ \{\bar{\boldsymbol{\tau}}\}_{j1} &= (\bar{\tau}_{xzj}(\beta,\gamma,h_j), \bar{\tau}_{yzj}(\beta,\gamma,h_j), \bar{\tau}_{zzj}(\beta,\gamma,h_j))^{\mathrm{T}}, \end{aligned} \tag{6}$$

Now, if vectors of the displacements and stresses are defined as

$$\{\bar{\mathbf{s}}\}_{j0} = \begin{Bmatrix} \{\bar{\mathbf{u}}\}_{j0} \\ \{\bar{\boldsymbol{\tau}}\}_{j0} \end{Bmatrix}, \qquad \{\bar{\mathbf{s}}\}_{j1} = \begin{Bmatrix} \{\bar{\mathbf{u}}\}_{j1} \\ \{\bar{\boldsymbol{\tau}}\}_{j1} \end{Bmatrix} \tag{7}$$

the expressions for them can be obtained as described below.

Since all displacements are time-harmonic, the Lamé equations for $j$th layer can be written as

$$\begin{aligned}
(\lambda_j + \mu_j)\frac{\partial \Delta_j}{\partial x} + \mu_j \nabla^2 u_j &= -\rho_j \omega^2 u_j \\
(\lambda_j + \mu_j)\frac{\partial \Delta_j}{\partial y} + \mu_j \nabla^2 v_j &= -\rho_j \omega^2 v_j \quad (j = 1, 2, \ldots, n+1), \\
(\lambda_j + \mu_j)\frac{\partial \Delta_j}{\partial z} + \mu_j \nabla^2 w_j &= -\rho_j \omega^2 w_j
\end{aligned} \tag{8}$$

where $\lambda_j$ and $\mu_j$ are Lamé constants of the $j$th layer, determined by

$$\lambda_j = \frac{\nu_j E_j (1 + \mathrm{i}\eta_j)}{(1 + \nu_j)(1 - 2\nu_j)}, \qquad \mu_j = \frac{E_j (1 + \mathrm{i}\eta_j)}{2(1 + \nu_j)}, \tag{9}$$

$$\Delta_j = \frac{\partial u_j}{\partial x} + \frac{\partial v_j}{\partial y} + \frac{\partial w_j}{\partial z} \tag{10}$$

is the dilatation, and $\nabla^2$ the Laplace operator.

The compression and shear-wave speeds of the $j$th layer are now denoted by

$$c_{j1} = \sqrt{\frac{(\lambda_j + 2\mu_j)}{\rho_j}}, \qquad c_{j2} = \sqrt{\frac{\mu_j}{\rho_j}} \quad (j = 1, 2, \ldots, n) \tag{11}$$

respectively, and the corresponding wave numbers as

$$k_{j1}^2 = \frac{\omega^2}{c_{j1}^2}, \quad k_{j2}^2 = \frac{\omega^2}{c_{j2}^2} \quad (j = 1, 2, \ldots, n). \tag{12}$$

By Fourier transforming equations (8) and (10), they become

$$\begin{aligned}
(\lambda_j + \mu_j)\mathrm{i}\beta \bar{\Delta}_j + \mu_j \left[ \frac{\mathrm{d}^2 \bar{u}_j}{\mathrm{d}z^2} - (\beta^2 + \gamma^2 - k_{j2}^2)\bar{u}_j \right] &= 0, \\
(\lambda_j + \mu_j)\mathrm{i}\gamma \bar{\Delta}_j + \mu_j \left[ \frac{\mathrm{d}^2 \bar{v}_j}{\mathrm{d}z^2} - (\beta^2 + \gamma^2 - k_{j2}^2)\bar{v}_j \right] &= 0, \\
(\lambda_j + \mu_j)\frac{\mathrm{d}\bar{\Delta}_j}{\mathrm{d}z} + \mu_j \left[ \frac{\mathrm{d}^2 \bar{w}_j}{\mathrm{d}z^2} - (\beta^2 + \gamma^2 - k_{j2}^2)\bar{w}_j \right] &= 0, \\
\bar{\Delta}_j = \mathrm{i}\beta \bar{u}_j + \mathrm{i}\gamma \bar{v}_j \rightarrow \frac{\mathrm{d}\bar{w}_j}{\mathrm{d}z}
\end{aligned} \tag{13, 14}$$

respectively. From equations (13) and (14),

$$\frac{\mathrm{d}^2 \bar{\Delta}_j}{\mathrm{d}z^2} - (\beta^2 + \gamma^2 - k_{j1}^2)\bar{\Delta}_j = 0. \tag{15}$$

Equation (15) represents the propagation of dilatational waves in the medium only. The solution to this differential equation can be obtained and hence also the full set of equations (13) which together represent the propagation of the dilatational waves (P-waves) and also the vertically and horizontally polarized shear waves (SH and SV waves).

The transformed stresses are determined from the Fourier transform of the stress–strain relation of the material, i.e.,

$$\begin{aligned}\bar{\tau}_{xzj} &= \mu_j(\mathrm{i}\beta\bar{w}_j + \mathrm{d}\bar{u}_j/\mathrm{d}z),\\ \bar{\tau}_{yzj} &= \mu_j(\mathrm{i}\gamma\bar{w}_j + \mathrm{d}\bar{v}_j/\mathrm{d}z),\\ \bar{\tau}_{zzj} &= (\lambda_j\bar{\Delta}_j + 2\mu_j\,\mathrm{d}\bar{w}_j/\mathrm{d}z).\end{aligned} \tag{16}$$

Using these definitions the solutions for the Fourier-transformed displacements and stresses at the upper and lower surfaces of a layer may be expressed in matrix form as

$$\{\bar{\mathbf{s}}\}_{j0} = [\mathbf{A}]_{j0}\{\mathbf{b}\}_j, \tag{17}$$

$$\{\bar{\mathbf{s}}\}_{j1} = \mathrm{e}^{\alpha_{j1}h_j}[\mathbf{A}]_{j1}\{\mathbf{b}\}_j, \tag{18}$$

where the integration constants, representing the participation of P, SV and SH waves travelling in two directions are accounted for in the vector $\{\mathbf{b}\}_j \in C^6$. $[\mathbf{A}]_{j0}$, $[\mathbf{A}]_{j1}$ are matrices of which the detailed expressions are given in Appendix A, with

$$\alpha_{j1}^2 = \beta^2 + \gamma^2 - k_{j1}^2,\ \alpha_{j2}^2 = \beta^2 + \gamma^2 - k_{j2}^2 \quad (j = 1, 2, \ldots, n). \tag{19}$$

From equations (17) and (18) it can be seen that $\alpha_{j1}$ and $\alpha_{j2}$ correspond to the complex decay constants, or wave numbers, applying in the vertical direction.

The combination of equations (17) and (18) links the displacements and stresses at the bottom of the layer with those at the top. This is the approach taken by Haskell and Thomson [15, 16] to define the layer 'transfer' matrix

$$\{\bar{\mathbf{s}}\}_{j1} = \mathrm{e}^{\alpha_{j1}h_j}[\mathbf{A}]_{j1}[\mathbf{A}]_{j0}^{-1}\{\bar{\mathbf{s}}\}_{j0}. \tag{20}$$

### 2.2.2. *The global analysis of the n layers*

The requirement for continuity of displacements and equilibrium of stresses at the layer interfaces is expressed by $\{\bar{\mathbf{s}}\}_{11} = \{\bar{\mathbf{s}}\}_{20}$, $\{\bar{\mathbf{s}}\}_{21} = \{\bar{\mathbf{s}}\}_{30}, \ldots, \{\bar{\mathbf{s}}\}_{n-1,1} = \{\bar{\mathbf{s}}\}_{n,0}$, so that

$$\begin{aligned}\{\bar{\mathbf{s}}\}_{n1} &= \mathrm{e}^{\alpha_{n1}h_n}[\mathbf{A}]_{n1}[\mathbf{A}]_{n0}^{-1}\{\bar{\mathbf{s}}\}_{n0} = \mathrm{e}^{\alpha_{n1}h_n}[\mathbf{A}]_{n1}[\mathbf{A}]_{n0}^{-1}\{\bar{\mathbf{s}}\}_{n-1,1}\\ &= \mathrm{e}^{\alpha_{n1}h_n}\mathrm{e}^{\alpha_{n-1,1}h_{n-1}}[\mathbf{A}]_{n1}[\mathbf{A}]_{n0}^{-1}[\mathbf{A}]_{n-1,1}[\mathbf{A}]_{n-1,0}^{-1}\{\bar{\mathbf{s}}\}_{n-1,0}\\ &\vdots\\ &= \mathrm{e}^{\sum_{j=1}^{n}\alpha_{j1}h_j}[\mathbf{A}]_{n1}[\mathbf{A}]_{n0}^{-1}[\mathbf{A}]_{n-1,1}[\mathbf{A}]_{n-1,0}^{-1}\cdots[\mathbf{A}]_{11}[\mathbf{A}]_{10}^{-1}\{\bar{\mathbf{s}}\}_{10}.\end{aligned} \tag{21}$$

Following the Haskell–Thomson method, a transfer matrix can be defined:

$$[\mathbf{T}] = \begin{bmatrix} [\mathbf{T}]_{11} & [\mathbf{T}]_{12} \\ [\mathbf{T}]_{21} & [\mathbf{T}]_{22} \end{bmatrix} = [\mathbf{A}]_{n1}[\mathbf{A}]_{n0}^{-1}[\mathbf{A}]_{n-1,1}[\mathbf{A}]_{n-1,0}^{-1} \cdots [\mathbf{A}]_{11}[\mathbf{A}]_{10}^{-1}, \quad (22)$$

where $[\mathbf{T}]_{11}$, etc., are $3 \times 3$ matrices, and the displacements and stresses at the lowest interface can be expressed in terms of those at the surface as

$$\begin{Bmatrix} \{\bar{\mathbf{u}}\}_{n1} \\ \{\bar{\boldsymbol{\tau}}\}_{n1} \end{Bmatrix} = \mathrm{e}^{\sum_{j=1}^{n} \alpha_{j1} h_j} \begin{bmatrix} [\mathbf{T}]_{11} & [\mathbf{T}]_{12} \\ [\mathbf{T}]_{21} & [\mathbf{T}]_{22} \end{bmatrix} \begin{Bmatrix} \{\bar{\mathbf{u}}\}_{10} \\ \{\bar{\boldsymbol{\tau}}\}_{10} \end{Bmatrix}. \quad (23)$$

2.2.3. *Analysis of the half-space*

For the half-space, putting $j = n + 1$ in equations (19) and (12), one can get $\alpha_{n+1,1}, \alpha_{n+1,2}, k_{n+1,1}, k_{n+1,2}$. Putting $j = n + 1$ in equations (5) and (6), gives $\{\bar{\mathbf{u}}\}_{n+1,0}, \{\bar{\boldsymbol{\tau}}\}_{n+1,0}$, where $\{\bar{\mathbf{u}}\}_{n+1,0}, \{\bar{\boldsymbol{\tau}}\}_{n+1,0}$ stand for the Fourier transformed displacement vector and stress vector on the top of the half-space. The equivalent of equations (17), for the half-space are

$$\begin{aligned} \{\bar{\mathbf{u}}\}_{n+1,0} &= [\mathbf{R}]\{\mathbf{b}\}_{n=1}, \\ \{\bar{\boldsymbol{\tau}}\}_{n+1,0} &= [\mathbf{S}]\{\mathbf{b}\}_{n+1}, \end{aligned} \quad (24)$$

where $\{\mathbf{b}\}_{n+1}$ are integration constants, $[\mathbf{R}]$ and $[\mathbf{S}]$ are $3 \times 3$ matrices of which the detailed expressions are given in Appendix A.

Equation (24) leads to the following to express the displacements in terms of the stresses at the upper surface of the half-space:

$$\{\bar{\mathbf{u}}\}_{n+1,0} = [\mathbf{R}][\mathbf{S}]^{-1}\{\bar{\boldsymbol{\tau}}\}_{n+1,0}. \quad (25)$$

2.2.4. *Expression of* $[\bar{\boldsymbol{\delta}}(\beta, \gamma)]$

The flexibility matrix for the layered ground system takes different forms depending on the nature of the lowest interface. Three cases are possible:

(i) *A half-space substratum*: Continuity of displacements and equilibrium of stresses at the interface of the layers and the half-space requires $\{\bar{\mathbf{u}}\}_{n+1,0} = \{\bar{\mathbf{u}}\}_{n1}$, $\{\bar{\boldsymbol{\tau}}\}_{n+1,0} = \{\bar{\boldsymbol{\tau}}\}_{n1}$, hence equation (25) becomes

$$\{\bar{\mathbf{u}}\}_{n1} = [\mathbf{R}][\mathbf{S}]^{-1}\{\bar{\boldsymbol{\tau}}\}_{n1}. \quad (26)$$

The substitution of equation (25) into equation (23) yields

$$\{\bar{\mathbf{u}}\}_{10} = ([\mathbf{R}][\mathbf{S}]^{-1}[\mathbf{T}]_{21} - [\mathbf{T}]_{11})^{-1}([\mathbf{T}]_{12} - [\mathbf{R}][\mathbf{S}]^{-1}[\mathbf{T}]_{22})\{\bar{\boldsymbol{\tau}}\}_{10}.$$

Putting

$$[\mathbf{Q}] = \begin{bmatrix} Q_{11} & Q_{12} & Q_{13} \\ Q_{21} & Q_{22} & Q_{23} \\ Q_{31} & Q_{32} & Q_{33} \end{bmatrix} = ([\mathbf{R}][\mathbf{S}]^{-1}[\mathbf{T}]_{21} - [\mathbf{T}]_{11})^{-1} \times ([\mathbf{T}]_{12} - [\mathbf{R}][\mathbf{S}]^{-1}[\mathbf{T}]_{22}) \tag{27}$$

yields the flexibility matrix of a layered ground with a half-space substratum

$$\{\bar{\mathbf{u}}\}_{10} = \begin{bmatrix} Q_{11} & Q_{12} & Q_{13} \\ Q_{21} & Q_{22} & Q_{23} \\ Q_{31} & Q_{32} & Q_{33} \end{bmatrix} \{\bar{\boldsymbol{\tau}}\}_{10}. \tag{28}$$

At this point the term $e^{\Sigma_{j=1}^{n} \alpha_{j1} h_j}$, which will be very large when $h_j$ is large, disappears in equations (27) and (28) and numerical difficulties are avoided.

(2) *A rigid foundation, no half-space*: In this case $\{\bar{\mathbf{u}}\}_{n+1,0} = \{\bar{\mathbf{u}}\}_{n1} = 0$, and from equation (23)

$$\{\bar{\mathbf{u}}\}_{10} = -[T]_{11}^{-1}[\mathbf{T}]_{12}\{\bar{\boldsymbol{\tau}}\}_{10} = [\mathbf{Q}]\{\bar{\boldsymbol{\tau}}\}_{10}, \tag{29}$$

where

$$[\mathbf{Q}] = -[\mathbf{T}]_{11}^{-1}[\mathbf{T}]_{12}. \tag{30}$$

(3) *The ground is represented only as a half-space*: When the ground is just a half-space (i.e. the case where $n = 0$), equation (25) is used, i.e.,

$$\{\bar{\mathbf{u}}\}_{10} = [\mathbf{R}][\mathbf{S}]^{-1}\{\bar{\boldsymbol{\tau}}\}_{10} = [\mathbf{Q}]\{\bar{\boldsymbol{\tau}}\}_{10}, \tag{31}$$

where

$$[\mathbf{Q}] = [\mathbf{R}][\mathbf{S}]^{-1}. \tag{32}$$

Now comparing equations (28), (29) or (31) with equation (4), gives

$$[\bar{\boldsymbol{\delta}}(\beta, \gamma)] = \begin{bmatrix} -Q_{11} & -Q_{12} & -Q_{13} \\ -Q_{21} & -Q_{22} & -Q_{23} \\ -Q_{31} & -Q_{32} & -Q_{33} \end{bmatrix}. \tag{33}$$

The minus signs in the matrix of equation (3) reflect the fact that the positive direction of normal stress on the surface of the ground, from the railway track, is defined as opposite to the $z$ direction.

From equation (27), the Fourier-transformed dynamic flexibility matrix may be derived when $n$ layers overly a half-space: from equation (30) the matrix may be derived when $n$ layers overly a rigid foundation; and from equation (32) the matrix may be derived when the ground is just a half-space. These dynamic flexibility

matrices are formulated only with $[\mathbf{A}]_{j0}$, $[\mathbf{A}]_{j1}$, and/or $[\mathbf{R}]$, $[\mathbf{S}]$. Examination of the expressions for these matrices, given in Appendix A, shows that no terms involve exponents where the real part is a positive value times the layer depth, $h_j$ since $\mathrm{Re}(\alpha_{j1}) > \mathrm{Re}(\alpha_{j2})$ because the dilational wave speed, $c_{j1}$, is greater than the shear wave speed, $c_{j2}$, in each layer. No numerical difficulties are therefore encountered for large layer thickness.

### 2.3. SOME PROPERTIES OF $Q_{13}(\beta, \gamma)$, $Q_{23}(\beta, \gamma)$, $Q_{33}(\beta, \gamma)$

It is worth noting some properties of $Q_{13}(\beta, \gamma)$, $Q_{23}(\beta, \gamma)$, $Q_{33}(\beta, \gamma)$ that lead to efficiencies in the calculation. These are

(1) $Q_{13}(\beta, \gamma)$ is an odd function of $\beta$, and an even function of $\gamma$.
(2) $Q_{23}(\beta, \gamma)$ is an even function of $\beta$, and an odd function of $\gamma$.
(3) $Q_{33}(\beta, \gamma)$ is an even function of $\beta$ and $\gamma$.
(4) By putting $\beta = \rho \cos\phi$, $\gamma = \rho \sin\phi$ (therefore $\rho = \sqrt{\beta^2 + \gamma^2}$, $\phi = \tan^{-1} \gamma/\beta$), then

$$Q_{13}(\beta, \gamma) = Q_{23}(0, \rho)\cos\phi$$

$$Q_{23}(\beta, \gamma) = Q_{23}(0, \rho)\sin\phi,$$

$$Q_{33}(\beta, \gamma) = Q_{33}(0, \rho). \tag{34}$$

The fourth property is very useful, because it reduces the calculation of matrix $[\mathbf{Q}]$ from a plane to an axis.

In order to calculate $[\mathbf{Q}]$ it is first necessary to calculate the matrix $[\mathbf{T}]$, while the calculation of $[\mathbf{T}]$ requires calculating the inverse of the matrices $[\mathbf{A}]_{j0}(j = 1, 2, \ldots, n)$ [equation (27)]. When $\beta = 0$, since there are many zero elements in the matrices $[\mathbf{A}]_{j0}$, the inverse of $[\mathbf{A}]_{j0}$ can be expressed analytically (omitted in this paper). The inverse matrix in equation (27) can also be expressed analytically because the matrix to be inverted is of order 3.

### 2.4. THE GROUND RESPONSE WHEN THE LOAD ACTS DIRECTLY ON THE SURFACE OF THE GROUND

Before considering the vibrational response of the ground to a load acting via a track, a few simple loading cases that have been the subject of previous work [4, 5, 7] are shown here. These cases are included briefly as they are useful for comparisons with the track loading case. In the following three subsections, the method of calculation is outlined for a rectangular or circular load, and an infinite strip load of finite width.

#### 2.4.1. *Vertical rectangular load*

Now $p_x = 0$, $p_y = 0$ for all points and $p_z = P_0/4ab$ when $-a \leqslant x \leqslant a$ and $-b \leqslant y \leqslant b$, and $p_z = 0$ at other points. This gives $\bar{p}_x = 0$, $\bar{p}_y = 0$,

$\bar{p}_z = (\sin \beta a/\beta a)(\sin \gamma b/\gamma b) P_0$, and substituting them into equation (4) yields,

$$\bar{u}_{10}(\beta, \gamma) = -Q_{13}(\beta, \gamma) \frac{\sin \beta a}{\beta a} \frac{\sin \gamma b}{\gamma b} P_0,$$

$$\bar{v}_{10}(\beta, \gamma) = -Q_{23}(\beta, \gamma) \frac{\sin \beta a}{\beta a} \frac{\sin \gamma b}{\gamma b} P_0,$$

$$\bar{w}_{10}(\beta, \gamma) = -Q_{33}(\beta, \gamma) \frac{\sin \beta a}{\beta a} \frac{\sin \gamma b}{\gamma b} P_0. \tag{35}$$

2.4.2. *Vertical circular load*

In this case $p_x = 0$, $p_y = 0$ for all points and $p_z = p_0/\pi R^2$ when $x^2 + y^2 \leqslant R^2$, and $p_z = 0$ at other points. Because the load is axisymmetric, it is convenient to use a polar co-ordinate system. It can be shown that the displacements of the point on the $y$-axis of the ground surface are as follows:

$$u_{10}(0, y) = 0,$$

$$v_{10}(0, y) = -\frac{\mathrm{i} P_0}{\pi R} \int_0^\infty Q_{23}(0, \rho) \mathrm{J}_1(\rho R) \mathrm{J}_1(\rho y) \, \mathrm{d}\rho$$

$$w_{10}(0, y) = -\frac{P_0}{\pi R} \int_0^\infty Q_{33}(0, \rho) \mathrm{J}_1(\rho R) \mathrm{J}_0(\rho y) \, \mathrm{d}\rho, \tag{36}$$

where $\mathrm{J}_0(y)$ and $\mathrm{J}_1(y)$ are Bessel functions of the first type and order 0 and 1.

2.4.3. *Vertical strip load aligned in x direction*

Now $p_x = 0$, $p_y = 0$ for all points and $p_z = P_0/2b$ when $-b \leqslant y \leqslant b$ and $p_z = 0$ at other points. One can show that $\bar{p}_x = 0$, $\bar{p}_y = 0$, $\bar{p}_z = 2\pi P_0 (\sin \gamma b/\gamma b) \delta(\beta)$, where $\delta(\beta)$ is the Dirac-$\delta$ function. Substituting them into equation (4) and doing an inverse Fourier transform, yields

$$u_{10}(x, y) = 0,$$

$$v_{10}(x, y) = -\frac{P_0}{2\pi} \int_{-\infty}^\infty Q_{23}(0, \gamma) \frac{\sin \gamma b}{\gamma b} \mathrm{e}^{\mathrm{i}\gamma y} \, \mathrm{d}\gamma,$$

$$w_{10}(x, y) = -\frac{P_0}{2\pi} \int_{-\infty}^\infty Q_{33}(0, \gamma) \frac{\sin \gamma b}{\gamma b} \mathrm{e}^{\mathrm{i}\gamma y} \, \mathrm{d}\gamma, \tag{37}$$

which can be written as

$$u_{10}(x, y) = 0,$$

$$v_{10}(x, y) = -\frac{iP_0}{\pi}\int_0^\infty Q_{23}(0, \gamma)\frac{\sin \gamma b}{\gamma b}\sin \gamma y \, d\gamma,$$

$$w_{10}(x, y) = -\frac{P_0}{\pi}\int_0^\infty Q_{33}(0, \gamma)\frac{\sin \gamma b}{\gamma b}\cos \gamma y \, d\gamma. \tag{38}$$

Equation (37) shows that the displacements are independent of $x$, the problem is of plane strain, and the Fourier transformed displacements of the ground surface are

$$\bar{u}_{10}(\gamma) = 0,$$

$$\bar{v}_{10}(\gamma) = -Q_{23}(0, \gamma)\frac{\sin \gamma b}{\gamma b}P_0,$$

$$\bar{w}_{10}(\gamma) = -Q_{33}(0, \gamma)\frac{\sin \gamma b}{\gamma b}P_0. \tag{39}$$

## 3. COUPLING OF THE GROUND AND THE RAILWAY

The railway is aligned in the $x$ direction and has a contact width $2b$ with the ground. Different railway structures may be represented by different models having the same form. As an example, a track structure comprising rail, rail pad, sleeper and ballast is presented. The rails are represented as a single beam and the rail pads are modelled as a distributed vertical stiffness (see Figure 1). The sleepers are modelled as a continuous mass per unit length of the track and the ballast is modelled as a continuous distributed vertical spring stiffness and mass.

A harmonic load $P_0 e^{i\omega t}$ acts on the head of the rails at a point just above the origin point $O$. The displacement of the rail in the $z$ direction is denoted by $w_1(x)$, that of the sleeper by $w_2(x)$, and the ballast/ground interface at the track centre line (i.e., the $x$-axis) by $w_3(x)$. The forces between the rail and the sleeper, the sleeper and the ballast, and at the ballast/ground interface are denoted by $F_1$, $F_2$ and $F_3$.

Representing the rails as a single Euler beam, the force balance equation, in the vertical direction, is

$$EI\frac{\partial^4 w_1}{\partial x^4} + m_R \ddot{w}_1 + F_1 = P_0 e^{i\omega t}\delta(x). \tag{40}$$

where $EI$ is the bending stiffness of the rails and $m_R$ is the mass of the rails per unit length of the track.

For sleepers, the force balance equation is

$$m_s \ddot{w}_2 - F_1 + F_2 = 0, \tag{41}$$

where $m_s$ is the distributed mass of the sleepers per unit length of track; the mass of the pads is neglected. $F_1 = k_P(w_1 - w_2)$, where $k_P$ is the vertical linear spring stiffness of the rail pads per unit length of track.

For the ballast, a vertical linear spring stiffness is assumed and the effects of inertia are included using the consistent mass approximation. This leads to

$$\frac{m_B}{6}\begin{bmatrix} 2 & 1 \\ 1 & 2 \end{bmatrix}\begin{Bmatrix} \ddot{w}_2 \\ \ddot{w}_3 \end{Bmatrix} + k_B\begin{bmatrix} 1 & -1 \\ -1 & 1 \end{bmatrix}\begin{Bmatrix} w_2 \\ w_3 \end{Bmatrix} + \begin{Bmatrix} -F_2 \\ F_3 \end{Bmatrix} = 0, \tag{42}$$

where $m_B$ is the mass, and $k_B$ is the spring stiffness of the ballast per unit length of track.

For the ground, only the normal contact force at the interface between the ballast and the ground is taken into account. This force is assumed to be constant in the $y$ direction from $y = -b$ to $y = b$ and has a strength per unit length in the $x$ direction of $F_3(x)e^{i\omega t}$ (so, the normal stress in the contact plane is $(F_3(x)/2b)\,e^{i\omega t}$).

Assembling equations (40)–(42) for the railway, assuming steady state harmonic solutions of circular frequency $\omega$, and Fourier transforming them with respect to $x$, leads to

$$\begin{bmatrix} EI\beta^4 - \omega^2 m_R + k_P & -k_P & 0 \\ -k_P & k_P + k_B - \omega^2(m_S + m_B/3) & -(k_B + \omega^2 m_B/6) \\ 0 & -(k_B + \omega^2 m_B/6) & (k_B - \omega^2 m_B/3) \end{bmatrix}\begin{Bmatrix} \bar{w}_1(\beta) \\ \bar{w}_2(\beta) \\ \bar{w}_3(\beta) \end{Bmatrix}$$

$$= \begin{Bmatrix} P_0 \\ 0 \\ -\bar{F}_3(\beta) \end{Bmatrix}. \tag{43}$$

Hysteretic damping is accounted for in the rail pad and the ballast by deriving complex stiffness properties using a loss factor in each case. The bar notation is again used to indicate the Fourier-transformed displacements and forces, i.e., $\bar{w}_1(\beta) = \int_{-\infty}^{\infty} w_1(x)e^{-i\beta x}\,dx$, $\bar{F}_3(\beta) = \int_{-\infty}^{\infty} F_3(x)\,e^{-i\beta x}\,dx$. The minus sign on the right-hand side of the third equation of equation (43) indicates that the force exerted at the bottom of the track structure by the ground is upward.

Continuity of the displacement at the ground surface is expressed as

$$w_3(x) = w_{10}(x, y = 0) = \frac{1}{4\pi^2}\int_{-\infty}^{\infty}\int_{-\infty}^{\infty} \bar{w}_{10}(\beta, \gamma)e^{i\beta x}\,d\beta\,d\gamma \tag{44}$$

from which

$$\bar{w}_3(\beta) = \int_{-\infty}^{\infty} w_3(x)e^{-i\beta x}\,dx = \frac{1}{2\pi}\int_{-\infty}^{\infty} \bar{w}_{10}(\beta, \gamma)\,d\gamma. \tag{45}$$

The following loads are applied at the ground surface (the $e^{i\omega t}$ term is omitted):

$$p_x = 0,$$

$$p_y = 0,$$

$$p_z = \begin{cases} F_3(x)/2b & \text{when } |y| \leqslant b, \\ 0, & \text{elsewhere,} \end{cases} \tag{46}$$

so that

$$\bar{p}_x = 0, \qquad \bar{p}_y = 0, \qquad \bar{p}_z(\beta, \gamma) = \frac{\sin \gamma b}{\gamma b} \bar{F}_3(\beta). \tag{47}$$

With the substitution of equation (47) into equation (4)

$$\bar{w}_{10}(\beta, \gamma) = -Q_{33}(\beta, \gamma) \frac{\sin \gamma b}{\gamma b} \bar{F}_3(\beta) \tag{48}$$

and by the substitution of equation (47) into equation (45),

$$\bar{w}_3(\beta) = \left( -\frac{1}{2\pi} \int_{-\infty}^{\infty} Q_{33}(\beta, \gamma) \frac{\sin \gamma b}{\gamma b} \, \mathrm{d}\gamma \right) \bar{F}_3(\beta) = \bar{H}(\beta) \bar{F}_3(\beta). \tag{49}$$

The integrand in the backeted term, defined by this equation as $\bar{H}(\beta)$, is even with respect to $\gamma$, so that

$$\bar{H}(\beta) = -\frac{1}{\pi} \int_0^{\infty} Q_{33}(\beta, \gamma) \frac{\sin \gamma b}{\gamma b} \, \mathrm{d}\gamma. \tag{50}$$

With the substitution of equation (49) into equation (43), $\bar{w}_1(\beta)$, $\bar{w}_2(\beta)$, $\bar{F}_3(\beta)$ can be obtained, and from equation (4)

$$\bar{u}_{10}(\beta, \gamma) = -Q_{13}(\beta, \gamma) \frac{\sin \gamma b}{\gamma b} \bar{F}_3(\beta),$$

$$\bar{v}_{10}(\beta, \gamma) = -Q_{23}(\beta, \gamma) \frac{\sin \gamma b}{\gamma b} \bar{F}_3(\beta),$$

$$\bar{w}_{10}(\beta, \gamma) = -Q_{33}(\beta, \gamma) \frac{\sin \gamma b}{\gamma b} \bar{F}_3(\beta). \tag{51}$$

The steady state displacements of the ground surface can be found by carrying out the inverse Fourier transform of equations (51).

## 4. CALCULATION EXAMPLES

In order to carry out example calculations, parameters for the ground have been taken from references [4, 7]. Results are presented for two ground models with the

TABLE 1

*The parameters for the ground*

| Layer | Depth (m) | Young's modulus ($10^6$N/m$^2$) | Possion ratio | Density (kg/m$^3$) | Loss factor | P-wave speed (m/s) | S-wave speed (m/s) |
|---|---|---|---|---|---|---|---|
| 1 | 2 or 7 | 269 | 0·257 | 1550 | 0·1 | 459 | 263 |
| Half-space | | 2040 | 0·179 | 2450 | 0·1 | 950 | 594 |

TABLE 2

*The parameters for the railway*

| | |
|---|---|
| Mass of rail beam per unit length of track | 120 kg/m |
| Bending stiffness of rail beam | $1{\cdot}26 \times 10^7$ N m$^2$ |
| Rail pad stiffness per unit length of track | $3{\cdot}5 \times 10^8$ N/m$^2$ |
| Rail pad loss factor | 0·15 |
| Mass of sleepers per unit length of track | 490 kg/m |
| Mass of ballast per unit length of track | 1200 kg/m |
| Ballast stiffness per unit length of track | $3{\cdot}15 \times 10^8$ N/m$^2$ |
| Loss factor of ballast | 1·0 |
| Contact width of railway and ground | 2·7 m |

same track. The material parameters of the two ground models are given in Table 1. The first ground model has a 7 m layer of soil with a stiffer half-space substratum. In the second case, the ground has the same material parameters except that the layer depth is only 2 m. Parameters for a typical railway track that have been used for both examples are presented in Table 2. The load has a unit amplitude and a frequency of 40 Hz.

For all the results presented, the inverse Fourier transform has been carried out using the FFT algorithm. An alternative is to use a numerical integration rule which takes account of the sine and cosine terms in the Fourier transform as its weighting functions. An adaptive integration rule based on the quadrature method of reference [17] has been used and found to be accurate and computationally efficient for obtaining results at a single $x, y$ location. However, for the present purpose of showing the results at a large number of locations on the surface, or for the purpose of implementing a summation of a large number of terms for vibration contributions from along the track [8], the fact that an FFT transforms a range of wave number points to a range of Cartesian co-ordinate locations simultaneously is advantageous. When using either integration technique, the domain of $\beta, \gamma$ for which the calculation is carried out prior to the inverse Fourier transform, must be chosen taking account of all the possible waves including those of the track structure. When the FFT is used, care must be taken to ensure that enough points

are transformed to constitute a sufficiently accurate quadrature. In this example, the FFT is carried out over a grid of $2048 \times 2048$ which covers a range of $-24/\text{m} < \beta, \gamma < 24/\text{m}$. Only $512 \times 512$ points of the transform are presented in the $x, y$ domain in the figures presented in this paper.

Figure 2 presents the vertical amplitude of displacement of the first ground model (7 m layer) in the wave number domain for a rectangular load 2.7 m × 2.7 m. At this frequency (40 Hz) a number of propagating modes may exist in the layer. Horizontally polarized shear wave (SH) motion is uncoupled from dilational (P) and vertically polarized shear wave motion (SV). For this reason, the SH modes (Love waves) are not relevant to the vertical displacement presented in the figure. The peaks in Figure 2 therefore correspond to different orders of P–SVmodes. (The peak corresponding to the highest wave speed, lowest wave number, represents the Rayleigh wave in the half-space.) P–SV modes are sometimes referred to as Rayleigh waves of differing order, or 'R-waves'. At high frequency, the speed of the first P–SV mode (highest wave number) of a layer approximates to the Rayleigh wave speed of a half-space of this material. This is indeed the case for the mode corresponding to the strongest peak at $(\beta^2 + \gamma^2)^{1/2} = 1{\cdot}03$ m in Figure 2.

The zero in amplitude for the wave number $\beta$ or $\gamma = 2{\cdot}3\ \text{m}^{-1}$ corresponds to the zero in the loading function (section 2.4.1) related to the width of the square loading patch. At this wave number a single wavelength fits across the width of the loading patch. The sum excitation of the ground across the loading patch is then zero.

Figure 3 presents the amplitudes of vertical displacement similar to Figure 2 but for the load applied via the coupled track structure. The zero can still be seen at

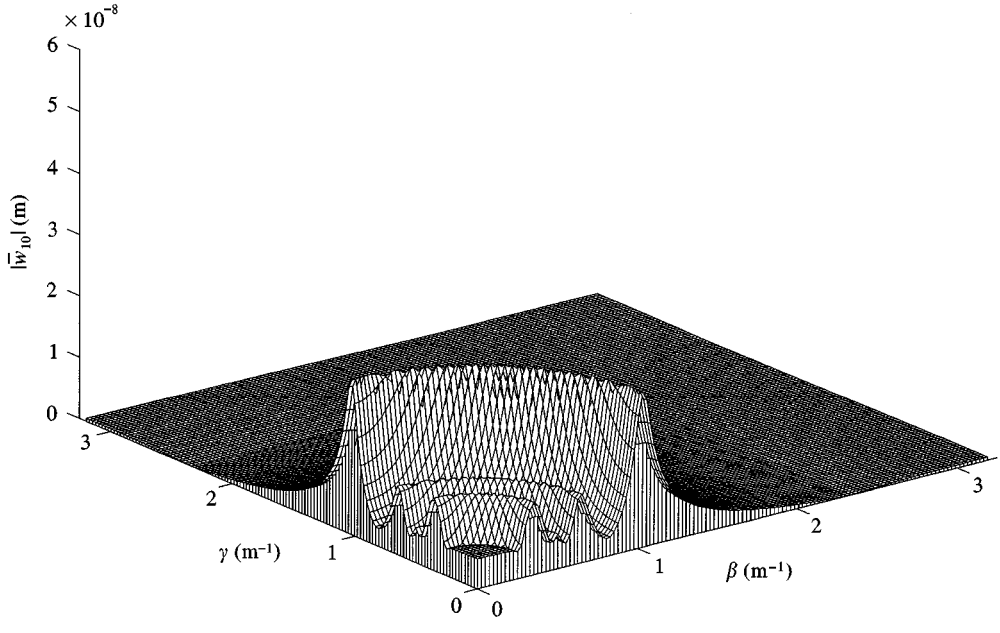


Figure 2. The amplitude of transformed vertical displacement of the ground surface: rectangular load at 40 Hz for the 7 m layer.

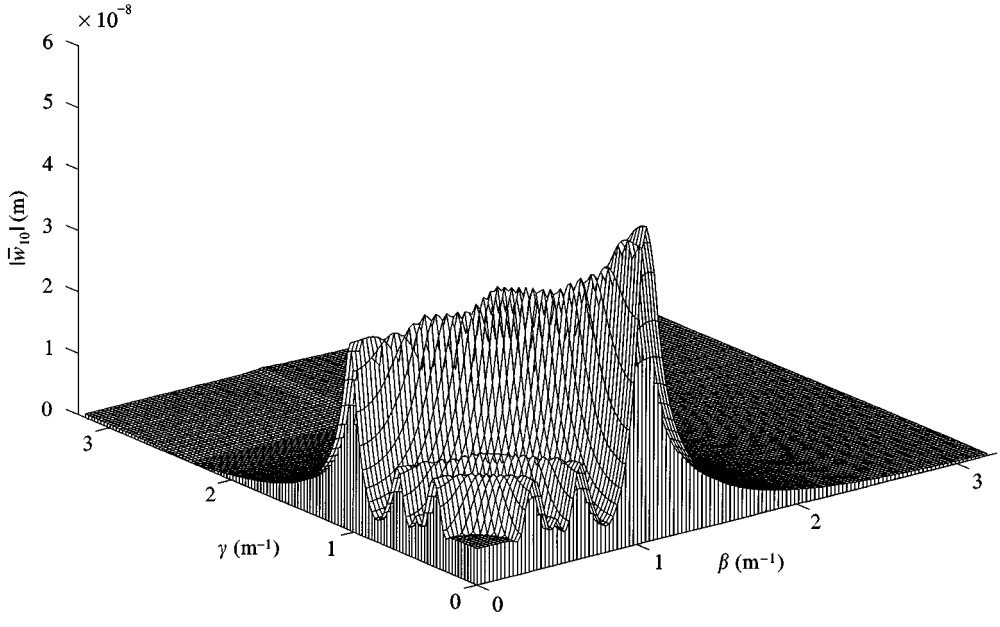


Figure 3. The amplitude of transformed vertical displacement of the ground surface: 40 Hz, with track for the 7 m layer.

$\gamma = 2{\cdot}3$ m because of the 2·7 m extent of the track in the $y$ direction. Indeed, the amplitudes of the waves travelling normal to the track, shown along the $\gamma$-axis, are very similar to those of the rectangular load. However, the amplitudes of the waves along the track, $\beta$-axis, are modified by its presence. In Figure 3, the first mode of propagation (i.e., highest wave number) is increased in amplitude from that indicated in Figure 2. With the track present, this peak corresponds to a mode in which the track acts as a beam on an elastic foundation. The position of the peak is therefore dependent on the mass and bending stiffness of the track structure. For a light track structure of low bending stiffness, the controlling stiffness and mass are those associated with the ground and the track wave number is close to the ground wave number. In Figure 3, neither the bending stiffness of the track (only that of the rail), nor its mass, are large enough to separate the peak for the track wave from that of the P–SV wave identified in Figure 2. There is therefore a single peak of greater amplitude in Figure 3. To demonstrate what happens for a more massive track structure the ballast mass has been increased to 3300 kg/m. In Figure 4, therefore, the track wave can be seen as the major carrier of vibrational energy in the $x$ direction, having, a peak distinct from the P–SV mode of the ground at a wave number of 1·3/m.

Figures 5–7 present, respectively, the vertical, lateral and longitudinal displacements of the ground surface for the load acting via the track (original ballast mass), as a function of $x$ and $y$. These figures all have the same vertical axis scale.

The effect of the track is to make both lateral and vertical displacement amplitudes greater along the line of the track than along the normal to it. The effects of a resonance of the track structure can be seen in both vertical and longitudinal

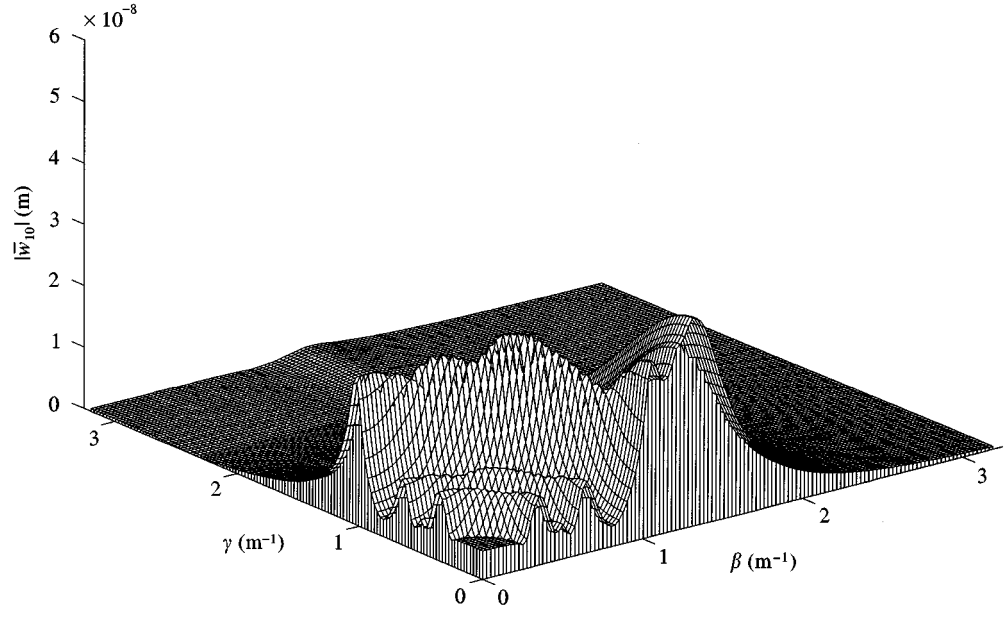


Figure 4. The amplitude of transformed vertical displacement of the ground surface: 40 Hz, heavier track, 7 m layer.

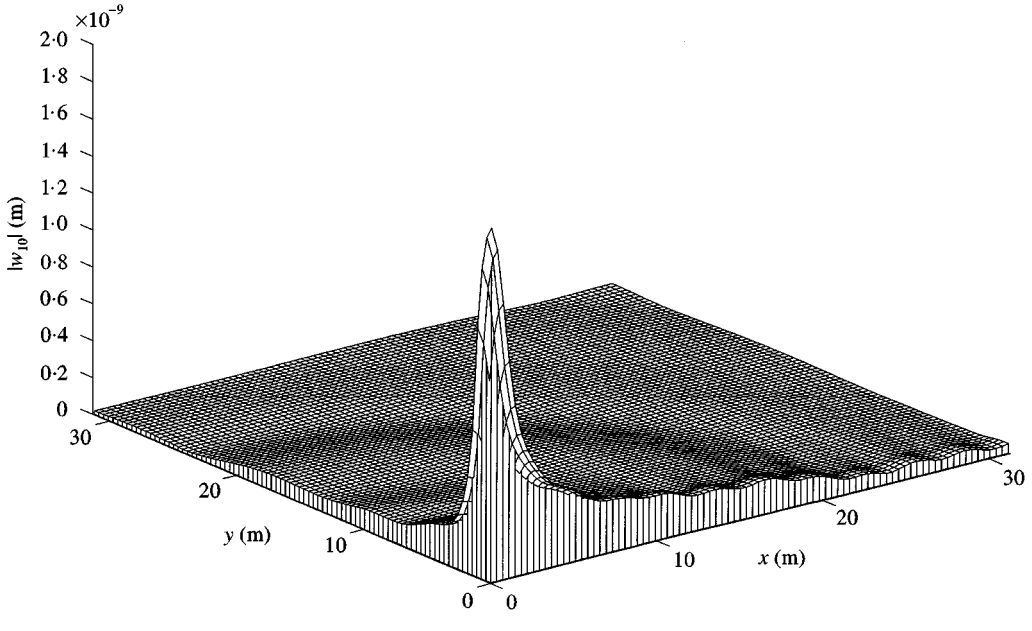


Figure 5. The amplitude of vertical displacement of the ground surface: 40 Hz, standard track, 7 m layer.

components along the $x$-axis. The vertical displacement amplitude drops quickly beyond the edge of the track, in the $y$ direction, but less quickly along the track. The lateral displacement amplitude is greatest near the edge of the track, being zero at the track centreline because of symmetry. Similarly, the longitudinal component

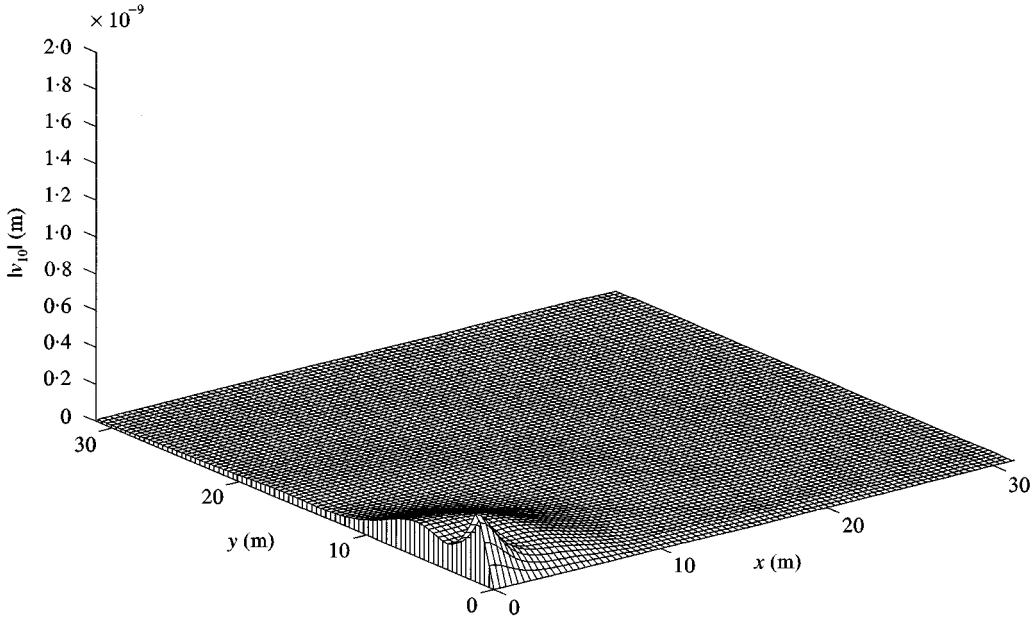


Figure 6. The amplitude of lateral displacement of the ground surface: 40 Hz, standard track, 7 m layer.

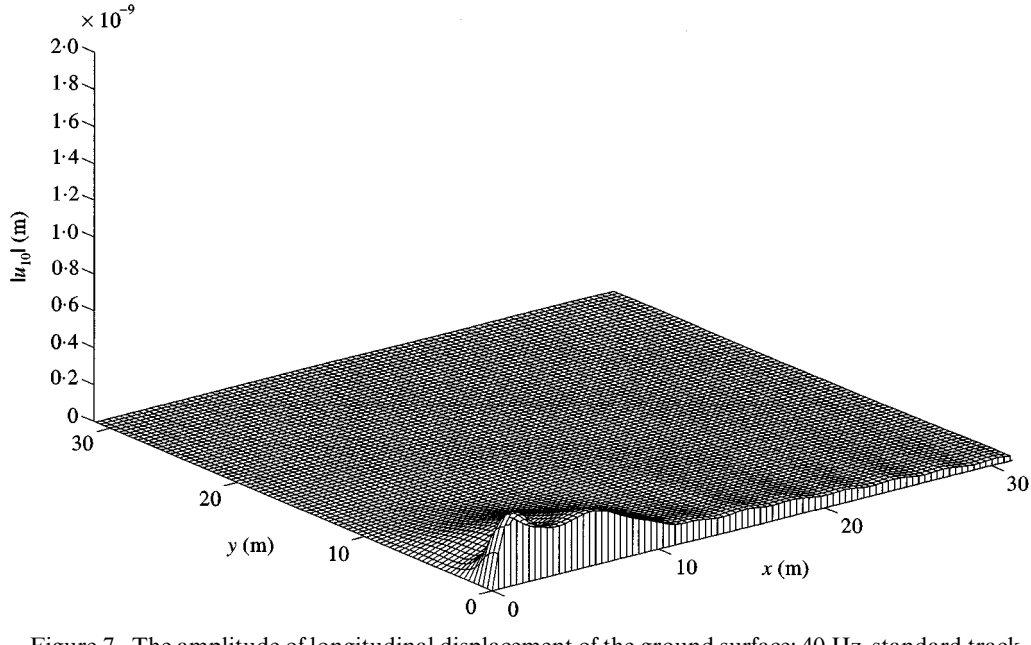


Figure 7. The amplitude of longitudinal displacement of the ground surface: 40 Hz, standard track, 7 m layer.

(Figure 7) is zero along the $y$-axis. Although the vertical load at the track obviously results in the vertical displacement being dominant near to its point of application, the transverse-lateral component of vibration becomes similar in amplitude to it from immediately to the side the track (at about $y = 2$ m) outwards. It can be seen

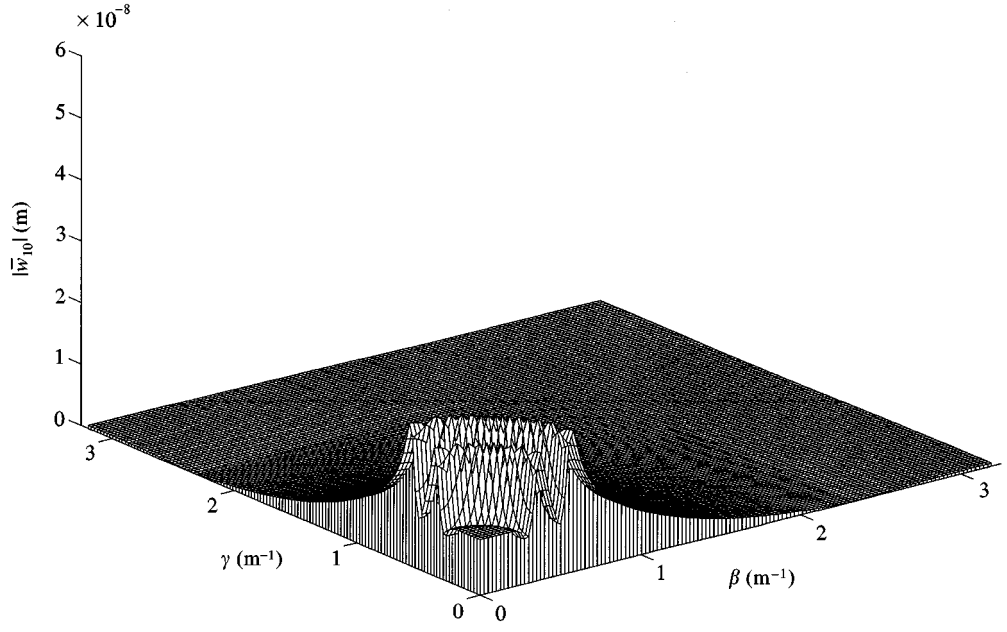


Figure 8. The amplitude of transformed vertical displacement of the ground surface: 40 Hz, rectangular load, 2 m layer.

that the longitudinal–lateral vibration component becomes similar in magnitude to the vertical component within a similar distance along the track.

Figure 8 presents the amplitude of vertical displacement of the surface of the ground with the 2 m layer in the wave number domain without the track. Zero amplitude can be seen at $\beta$ or $\gamma = 2{\cdot}3$ m corresponding to the zero in the loading function related to the contact width as found in Figure 2 for the 7 m layer ground. In Figure 8, two peaks can be seen corresponding to propagating waves at wave numbers $\beta$ or $\gamma = 0{\cdot}55$ and $0{\cdot}36$ m. Using the calculation method outlined in reference [5], the peak at $0{\cdot}55$ m has been identified as the Rayleigh wave in the lower half-space modified by the mass of the layer on top. This also coincides with the P-wave in the upper layer. The peak at 0.36 m corresponds to the only existing P–SV mode in the layer.

Figure 9 for the amplitude of vertical response in the wave number domain when the load acts via a track, shows the influence of the track wave. Since the lowest wave speed of the ground is at $\beta = 0{\cdot}55$ m, the track wave appears as an enhancement to the amplitude of this peak and the track wave is controlled by the P-wave in the layer and the Rayleigh wave in the substratum rather than a high order P–SV wave in the layer as was the case for the 7 m layer. The comparison of Figures 8 and 9 shows that, for all wave types, propagation along, and also in this case normal to, the track is increased in amplitude by the presence of the track. This is not the case for the track on the 7 m layer (Figure 3).

Figure 10 presents the amplitude of vertical displacement on the ground with the 2 m layer. This may be compared with Figure 5 for the ground with the 7 m layer,

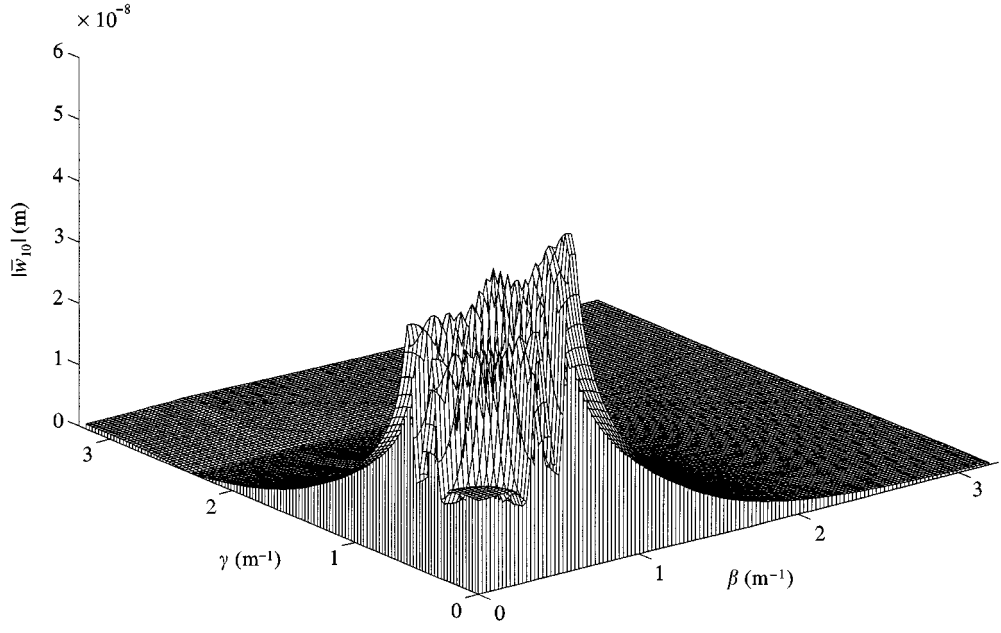


Figure 9. The amplitude of transformed vertical displacement of the ground surface: 40 Hz, standard trace, 2 m layer.

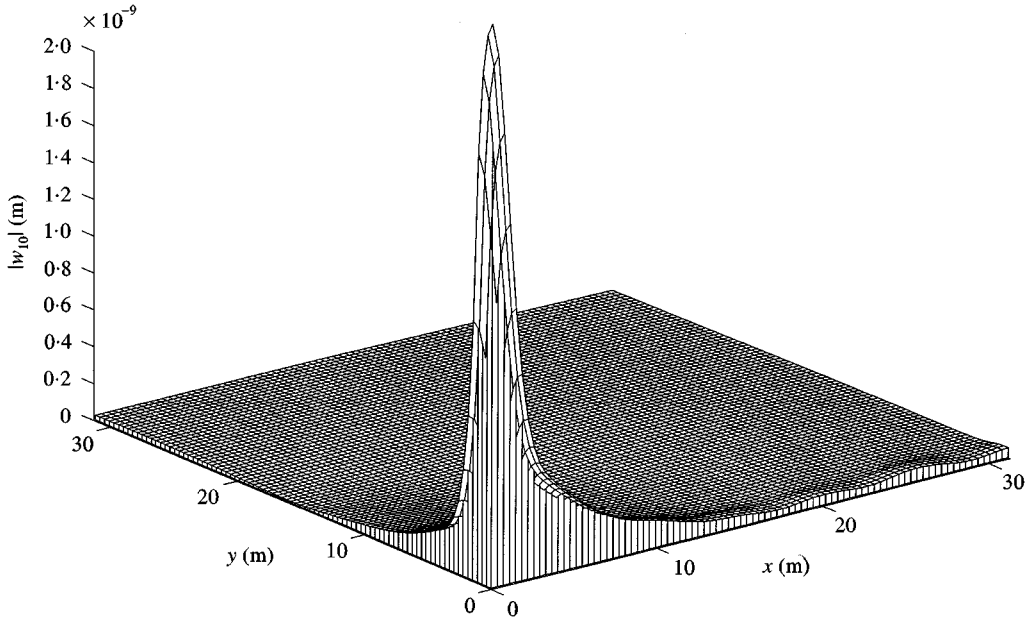


Figure 10. The amplitude of vertical displacement of the ground surface: 40 Hz, standard track, 2 m layer.

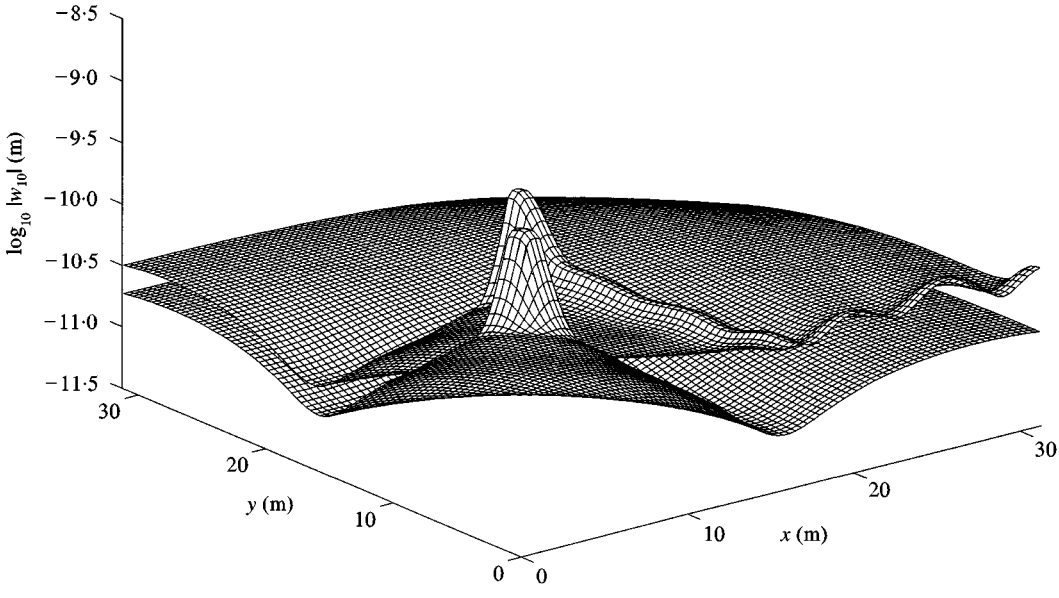


Figure 11. The amplitude of vertical displacement of the ground surface with the railway track (higher level on plot) and with the rectangular load (lower level on plot) at 40 Hz for the 2 m layer ground.

which is plotted to the same vertical scale. The amplitude at the loading point beneath the track is greater for the 2 m layer (Figure 10) than for the 7 m layer (Figure 5). However, a greater rate of attenuation with distance, both along, and normal to, the track, is shown in the 2 m layer ground. This occurs because the dominating amplitude at the surface is that of the P-wave in the layer.

Figure 11 presents the logarithm (base 10) of the vertical amplitude of vibration as a function of $x$ and $y$ for the rectangular load and for the track load on the same scale. The lower surface shown in this plot is for the rectangular load. It can been seen that the overall effect of the presence of the track is to increase the amplitude of vibration from the unit load by a factor of approximately 2 (0·3 on the log scale) within much of the distance range presented. A stronger effect under the track can be seen along the $x$-axis.

## 5. CONCLUSIONS

A method of calculation of the vibrational response of a layered ground subject to a fixed-position harmonic load acting via a railway track structure, or acting directly on the ground surface, has been produced. This can be used in the study of vibration induced dynamically due to the irregular vertical profile of the track and for vibration excited by lower speed vehicles (i.e., speeds well below the wave speeds in the ground). The method developed here is efficient and more accurate than a finite-element dynamic stiffness matrix approach that has been used previously for a similar model and so allows the responses at a large number of points to be

produced. A model for the effects of loads moving at high speeds is intended to be the subject of a subsequent paper by the present authors.

Example results have been produced for a railway track resting on two different ground models, the first having a 7 m layer on a stiffer half-space substratum and the second having a 2 m layer on the same substratum. Each model has been examined at a frequency of 40 Hz and it has been demonstrated that different regimes of wave propagation occur in the two cases. For the 7 m layer, vibration may be transmitted via a number of P–SV modes of the layer. A track wave exists which is associated with the lowest speed P–SV mode. For the 2 m layer the lowest wave speed occurs at the coincidence of the P-wave in the layer and the Rayleigh wave in the substratum. The track wave is therefore tied to this wave speed. The propagation regime of the 2 m layer ground leads to a higher rate of attenuation of vibration away from the loading point than for the 7 m layer. Both examples show a strong effect of the track structure on the amplitude and directivity of the vibration propagated, epecially in the field close to the track.

## ACKNOWLEDGMENT

C. J. C. Jones wishes to acknowledge the financial support of the EPSRC under research grant GR/L11397 for his participation in this work.

## REFERENCES

1. C. J. C. Jones 1996 *Better journey time—better business—Selected papers presented at "S-tech '96", IMechE, London*, 87–97. Reduction of noise and vibration from freight trains.
2. C. J. C. Jones 1994 *Proceedings of the Institution of Civil Engineers, Transportation* **105**, 43–51. Use of numerical models to determine the effectiveness of anti-vibration systems for railways.
3. D. V. Jones and M. Petyt 1991 *Journal of Sound and Vibration* **147**, 155–166. Ground vibration in the vicinity of a strip load: a two-dimensional half-space model.
4. D. V. Jones and M. Petyt 1993 *Journal of Sound and Vibration* **161**, 1–18. Ground vibration in the vicinity of a strip load: an elastic layer on half-space.
5. E. Kausel and J. M. Roësset 1981 *Bulletin of the Seismological Society of America* **71**, 1743–1761. Stiffness matrices for layered soils.
6. D. V. Jones and M. Petyt 1993 *Journal of Sound and Vibration* **166**, 141–159. Ground vibration in the vicinity of a rectangular load on a half space.
7. D. V. Jones and M. Petyt 1998 *Journal of Sound and Vibration* **212**, 61–74. Ground vibration due to a rectangular harmonic load.
8. C. J. C. Jones and J. R. Block 1996 *Journal of Sound and Vibration* **193**, 205–213. Prediction of ground vibration from freight trains.
9. G. Waas 1972 *Ph.D. Thesis, Department of Civil Engineering, University of California, Berkeley*. Linear two-dimensional analysis of soil dynamic problems in semi-infinite layered media.
10. J. L. Tassoulas and E. Kausel 1983 *International Journal for numerical methods in engineering* **19**, 1005–1032. Elements for the numerical analysis of wave motion in layered strata.
11. C. J. C. Jones 1996 *Proceedings of Internoise '96*, 412–426. Groundborne noise from new railway tunnels.

12. H. TAKEMIYA and K. GODA 1998 *Structural Engineering/Earthquake Engineering, JSCE* 605/I–45, 161–169. Wave propagation/impediment in a soil stratum over rigid base due to impulse/moving loads (in Japanese).
13. B. ALABI 1989 *Applied Mathematical Modelling* **13**, 710–715. A model for the problem of ground vibration induced by the wheels of moving train.
14. V. V. KRYLOV 1995 *Applied Acoustics* **44**, 149–164. Generation of ground vibration by superfast trains.
15. N. HASKELL 1953 *Bulletin of the Seismological Society of America* **73**, 17–43. The dispersion of surface waves on multilayered media.
16. W. T. THOMSON 1950 *Journal of Applied Physics* **21**, 81–93. Transmission of elastic waves through a stratified soil medium.
17. R. PIESSENS, E. DEDONCKER-KAPENGA, C. UBERHUBER and D. KAHANER 1983 *Quadpack: A Subroutine Package for Automatic Integration.* Series in Computational Mathematics. Berlin: Springer.

## APPENDIX A

When $\beta = 0$,
*Matrix* $[\mathbf{A}]_{j0} = (a_{kl})$ $(k, l = 1, 2, \ldots, 6;\ j = 1, 2, \ldots, n)$:

$$a_{12} = 1, \qquad a_{15} = 1, \qquad a_{23} = 1, \qquad a_{26} = 1,$$

$$a_{24} = a_{21}, \qquad a_{34} = -a_{31}, \qquad a_{36} = -a_{33}, \qquad a_{45} = -a_{42},$$

$$a_{54} = -a_{51}, \qquad a_{56} = -a_{53}, \qquad a_{64} = a_{61}, \qquad a_{66} = a_{63},$$

$$a_{21} = -\mathrm{i}\gamma/k_{j1}^2, \qquad a_{31} = -\alpha_{j1}/k_{j1}^2, \qquad a_{33} = -\mathrm{i}\gamma/\alpha_{j2}, \qquad a_{42} = \alpha_{j2}\mu_j,$$

$$a_{51} = -2\mathrm{i}\mu_j\alpha_{j1}\gamma/k_{j1}^2, \qquad a_{53} = \mu_j(\gamma^2/\alpha_{j2} + \alpha_{j2}),$$

$$a_{61} = -\mu_j(k_{j2}^2 + 2\alpha_{j2}^2)/k_{j1}^2, \qquad a_{63} = -2\mathrm{i}\mu_j\gamma$$

other $a$'s are zero.

*Matrix* $[\mathbf{A}]_{j1}$ $(j = 1, 2, \ldots, n)$:

$$[\mathbf{A}]_{j1} = [\mathbf{A}]_{j0}[\mathbf{D}]_j,$$

where $[\mathbf{D}]_j$ is a diagonal matrix with the elements of

$$d_{11} = 1, \qquad d_{22} = \mathrm{e}^{(\alpha_{j2} - \alpha_{j1})h_j}, \qquad d_{33} = d_{22}, d_{44} = \mathrm{e}^{-2\alpha_{j1}h_j},$$

$$d_{55} = \mathrm{e}^{-(\alpha_{j1} + \alpha_{j2})h_j}, \qquad d_{66} = d_{55}$$

*Matrix* [**R**] *and* [**S**]:

$$[\mathbf{R}] = \begin{bmatrix} 0 & 1 & 0 \\ -\dfrac{\mathrm{i}\gamma}{k_{n+1,1}^2} & 0 & 1 \\ \dfrac{\alpha_{n+1,1}}{k_{n+1,1}^2} & 0 & \dfrac{\mathrm{i}\gamma}{\alpha_{n+1,2}} \end{bmatrix},$$

$$[\mathbf{S}] = \begin{bmatrix} 0 & -\mu_{n+1}\alpha_{n+1,2} & 0 \\ \dfrac{2\,\mathrm{i}\mu_{n+1}\alpha_{n+1,1}\gamma}{k_{n+1,1}^2} & 0 & -\dfrac{\mu_{n+1}(\gamma^2+\alpha_{n+1,2}^2)}{\alpha_{n+1,2}} \\ \lambda_{n+1} - 2\mu_{n+1}\dfrac{\alpha_{n+1,1}^2}{k_{n+1,1}^2} & 0 & -2\mathrm{i}\mu_{n+1}\gamma \end{bmatrix}.$$